Eur. Phys. J. Appl. Phys. **44**, 21–28 (2008)
DOI: 10.1051/epjap:2008145

THE EUROPEAN PHYSICAL JOURNAL
APPLIED PHYSICS

Confocal microscopy of geometrically frustrated hard sphere crystals

R.P.A. Dullens[1], V.W.A. de Villeneuve[2,a], M.C.D. Mourad[2], A.V. Petukhov[2], and W.K. Kegel[2]

[1] Physical and Theoretical Chemistry Laboratory, Department of Chemistry, University of Oxford, South Parks Road, Oxford OX1 3QZ, UK
[2] Van 't Hoff Laboratory for Physical and Colloid Chemistry, Debye Institute, Utrecht University, Padualaan 8, 3584 CH Utrecht, The Netherlands

Received: 20 September 2007 / Received in final form: 9 May 2008 / Accepted: 16 June 2008
Published online: 22 July 2008 –

Abstract. Confocal microscopy has been used to study the crystallization of two colloidal model systems that are geometrically frustrated in a completely different way: (I) hard colloidal polyhedrals, where crystallization is frustrated due to the incommensurate particle shape and (II) large spherical impurities in a sea of monodisperse colloidal hard spheres, where crystallization is frustrated by the introduction of impurities. As a reference system, we analyzed the crystallization of pure monodisperse colloidal hard spheres. We show that although the crystal structures of both systems are highly dissimilar on the individual particle level, both sources of geometrical frustration have a similar effect on the structure on the grain level. We quantitatively characterize the polycrystalline structures and study the crystallization process in time. Whereas grain boundaries persist in the frustrated systems due to structural arrest, the majority of grain boundaries anneals out quite rapidly in the reference system. Therefore, we argue that both sources of geometrical frustration cause a polycrystalline structure.

PACS. 61.72.Mm Grain and twin boundaries – 61.82.Rx Nanocrystalline materials – 82.70.Dd Colloids

1 Introduction

Crystals are characterized by perfect periodic order. However, in practice crystals always exhibit various types of imperfections or defects such as vacancies, dislocations, stacking faults, grain boundaries and impurities [1]. Defects can for instance arise due to freezing in during crystal growth or as a result of stress on the crystal. Their presence strongly influences macroscopic properties of many materials like semiconductors, metals and ceramics [2]. For example, grain boundaries in crystals crucially influence the mechanical properties, as the grain size is directly related to the strength of materials [1–4]. For relatively small grain sizes the strength increases with increasing grain size [4–6], while for larger grain sizes the materials strengthens if the crystallites gets smaller (Hall-Petch effect) [7,8]. Therefore, controlling the grain size, for instance by tuning the solidification rate, heating or mechanical annealing, is of paramount importance in material science [1,3,9,10]. On the other hand, powders of small crystalline grains may have some degree of crystallinity in their superstructure. Here the extent of order is for example influenced by the roughness and the size distribution of the crystal grains.

Studying grain boundary formation and grain growth in atomic and molecular crystals in real-space and real-time is rather difficult due to the small length scales involved in atomic and molecular systems. Nevertheless, electron microscopy has provided much of the present experimental knowledge on grain boundaries [11–14]. However, it cannot be used to address the evolution of structures in real-time on the particle level in three dimensions. Consequently, computer simulations have proven to be beneficial to study these issues on the atomic level [15–21]. Inherent to their typical size, colloidal systems provide an excellent model tool to address these issues experimentally. In contrast to atomic systems, colloidal systems consist of particles with a characteristic size between a nanometer and several micrometers. This length scale makes them very suitable to be studied in real-space and real-time by microscopy techniques [22–24]. In particular, the combination of advanced colloidal particles and confocal microscopy has already made it possible to study several fundamental condensed matter problems, such as freezing, melting and glass formation, on the single-particle level [10,22–36]. Interestingly, colloidal systems exhibit similar phase-behaviour as atomic systems, making colloids a powerful model-system for condensed matter and atomic materials [37–40]. Furthermore, the interaction potential of colloids is tunable by e.g. adding

[a] e-mail: v.w.a.devilleneuve@uu.nl

polymers, which introduces an effective attraction between the colloids [41–43], or by increasing the surface charges to generate long-range repulsions [44]. Hence, this makes it possible to closely mimic atomic interaction potentials in colloidal systems [39,41–44].

In this work, we consider two colloidal model systems that exhibit completely different types of geometrical frustration: the crystals of the colloidal polyhedrals are frustrated due to incommensurate particle shape [45,46], while the crystals in the second system are frustrated by the addition of model impurities [32,34]. The influence of particle shape is e.g. relevant for applications in powder technology, ceramics [47], nanoparticles [48] and granular matter [49] where often a distribution of particle shapes is observed. The colloidal crystal containing impurities may serve as a model system for nanocrystalline materials containing dopants [19–21,50] and precipitates [51,52]. In our previous work we studied the structure of single crystalline domains of hard polyhedral colloids, without considering grain boundaries [45,46]. Furthermore, we addressed the influence of the presence of impurities on the dynamics of crystallization of colloidal hard spheres, without quantitatively analyzing the final crystal structure [32,34]. Here, we use real-space confocal microscopy [53] to quantitatively characterize the polycrystalline structure of geometrically frustrated colloidal crystals. The use of hard interactions allows the investigation of a single source of geometrical frustration. Our results clearly show that both sources of geometrical frustration – which are completely different in nature – significantly reduce the grain size of the colloidal crystals in a very similar way. In addition, we investigate the arrested grain growth by identifying the (time-dependent) defect-structure during grain growth.

2 Experimental

The '*polyhedral system*' consists of crosslinked and fluorescently labeled polymethyl methacrylate (PMMA) colloids that are monodisperse in size, but exhibit a polyhedral particle shape [45,54] (see Fig. 1A). In our experiments, we compare the polyhedrals to a reference system of spherical and size-monodisperse reference PMMA particles of equal size [55] (see Fig. 1B). The diameters d of the polyhedral and reference particles are respectively $d = 2.23 \pm 0.09$ and $d = 2.33 \pm 0.07$. The '*impurity system*' consists of a sea of fluorescently labeled monodisperse PMMA particles with a diameter d_p of 1.5 ± 0.09 μm containing a small fraction of very large PMMA particles, called the impurities [32,34]. The impurities were obtained by a synthesis following [55]. The resulting particles were extremely polydisperse and very large ($d_i \in$ 0.1–100 μm) as illustrated in Figure 1C. Impurities of different sizes were separated by repeated sedimentation. Subsequently a small amount (typically < 0.1 weight%) of impurities of the desired size was added to a sea of small PMMA particles. As a result, systems of monodisperse PMMA spheres contaminated with differently sized model impurities were obtained. Obviously, the reference system is formed by the same monodisperse PMMA spheres ($d_p = 1.5$ μm) without impurities. The impurity systems are characterized by the size ratio between the particles and the impurities $\alpha \equiv (d_i/d_p)$ m with d_i and d_p respectively the diameters of the impurity and the particles. In this work, we consider impurity systems with $\alpha = 5, 8, 13$ and 21, which covers ratios from impurity molecules up to objects of the size of precipitates.

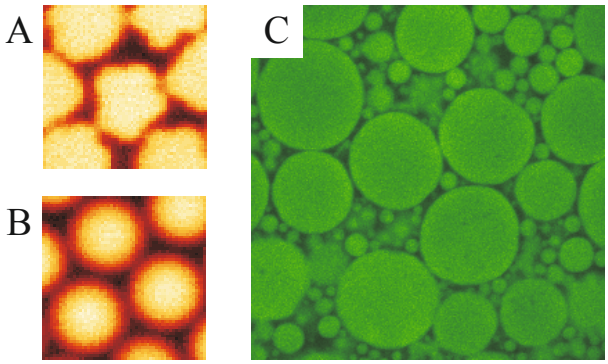

Fig. 1. (Color online) Confocal microscopy images of (A) the polyhedral particles and (B) the spherical reference particles (9×9 μm^2). (C) Confocal image of the impurities (70×70 μm^2) directly after synthesis. The larger particles (i.e. $d_i \in$ 7.5–31.5 μm) were used as model impurities in a sea of small monodisperse particles ($d_p = 1.5$ μm).

The colloidal model systems were dispersed in a mixture of cis-decalin (Merck, for synthesis), tetralin (Merck, for synthesis) and carbontetrachloride (Merck, for spectroscopy), which simultaneously matches the refractive index and almost the mass density of the particles [34,56]. In this solvent the particles interact via a hard-sphere-like potential [56,57]. The dispersions were contained in small homemade vials [56] and the particles were imaged using a Nikon TE 2000U inverted microscope with a Nikon C1 confocal scanning laser head. For the polyhedral colloids, samples with a volume fraction $\phi \equiv \rho v \approx 0.40$ were prepared (with ρ the number density and v the particle's volume). The impurity systems were prepared at relatively high volume fraction ($\phi \approx 0.55$) to minimize the mobility of the impurity during the measurements [32,34]. The volume fractions of the samples were defined relative to the random close packing density at the relevant polydispersity [58].

In the polyhedral, the impurity and the reference systems the colloidal crystal heterogeneously nucleates at the wall, followed by subsequent upward growth [32,34,36,59]. As a result, the (111)-plane of the crystal is oriented at the wall, allowing a quantitative 2D in-plane analysis of the systems [28,32,34,45,59,60]. The structure of the polyhedrals was analyzed after slow sedimentation had fully completed as the influence of the particle shape is most pronounced at highest compression. Since the layering in the polyhedral system did not persist in bulk [45], we studied the first layer at the glass wall in this system. Although certainly interesting, the question as to how the structure of the polyhedrals evolves in the third dimension lies outside the scope of this work. The impurity system

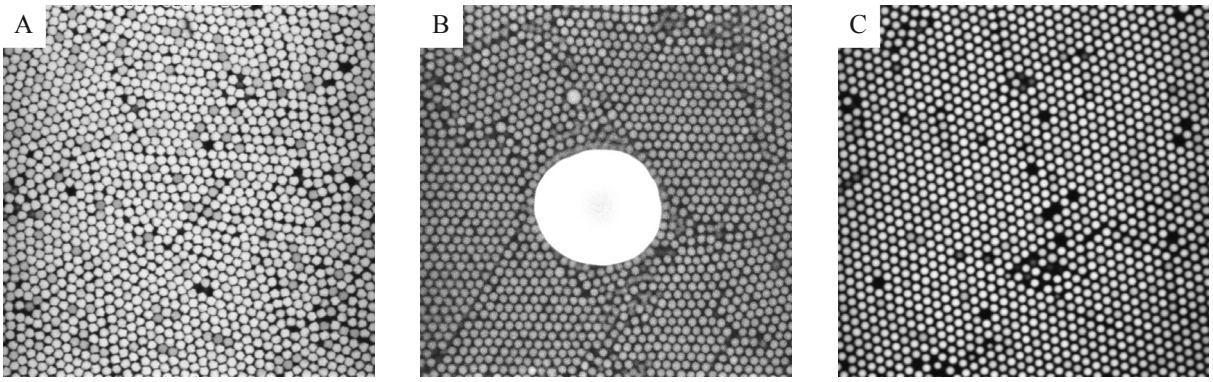

Fig. 2. Representative confocal images of (A) the polyhedrals (75×75 μm^2) and (B) the impurity system for $\alpha = 13$ (60×60 μm^2) and (C) the reference spheres for the polyhedrals (75×75 μm^2). The system without impurities is equivalent to the image shown in (C).

was studied in the plane corresponding to the center of the impurity, which was typically 20 μm above the glass wall. Furthermore, we studied the time-dependent structure of both systems during crystallization. The centers of the particles were located using image-analysis software similar to that described in [61]. We verified that the polyhedral particle shape did not significantly affect the accuracy of the particle tracking.

3 Results and discussion

Representative confocal micrographs of the colloidal crystal formed by the frustrated and reference systems are shown in Figure 2. The structure of both the polyhedrals and the impurity system exhibit a much higher degree of polycrystallinity compared to the structure formed by the reference spheres. To quantify this, we computed the radial distribution function $g(r)$ (being proportional to the probability of observing a particle a distance r away from a given particle):

$$g(r) = \frac{1}{\rho}\left\langle \sum_{j\neq i} \delta(r_i - r_j - r) \right\rangle. \qquad (1)$$

The indices i and j run over all particles. The radial distribution functions for the polyhedral, the impurity and the reference systems are shown in Figures 3A1 and 3B1. We observe for the polyhedrals that the peaks in the $g(r)$ are markedly broadened and that the structure in the $g(r)$ decays much faster with respect to the reference $g(r)$. Nevertheless, the clear differences between the $g(r)$ of the polyhedrals and the reference $g(r)$ are not due to polycrystallinity. The polyhedral particle-shape frustrates the hexagonal crystal on the single-particle level, leading to significant differences between the radial distribution functions [45]. Moreover, the differences in the radial distribution functions observed in Figure 3A1, are similar to those observed in single-crystalline regions [45]. Thus, the $g(r)$ is relatively insensitive to the presence of grain boundaries. This is corroborated by the impurity-$g(r)$, which appears to be rather similar to that of the reference system without impurities. Hence, in the impurity system the crystals are not frustrated on the particle level, leading to similar radial distribution functions for the impurity and reference system despite the presence of grain boundaries. Note that the difference between the reference radial distribution functions in Figures 3A1 and 3B1 is due to a difference in volume fraction. Recall that the polyhedral system has been analyzed after sedimentation had fully completed, in contrast to the impurity system. The volume fraction can be quantified in terms of the two-dimensional packing fractions ($\eta = N_T A_p / L^2$, with N_T the total number of particles in the image and L^2 the area of the image). Indeed, the more pronounced peaks in the reference $g(r)$ in Figure 3A1 (polyhedrals) correspond to a packing fraction of $\eta = 0.85$, which is clearly higher than $\eta = 0.74$ for the reference $g(r)$ in Figure 3B1 (impurity system).

The loss of positional order shows up strongly in reciprocal space. The 2D structure factor is computed on a 2D grid of $\boldsymbol{q}$-values with a sampling rate of π/L with L the size of the microscopic image, as in [46]:

$$S_{\boldsymbol{q}} = \frac{1}{N}\left|\sum_{n=1}^{N} \exp(i\boldsymbol{q}\,\boldsymbol{r}_n)\right| \qquad (2)$$

with $\boldsymbol{r}_n$ the particle coordinates and N the total number of particles. The structure factor profile $S(q)$ and the $g(r)$ profile are two related but distinctly different representations. As will be shown in more detail below, the $S(q)$ is more convenient for quantitative characterization of various types of long-range positional disorder, which is hidden in the details of the decay of the higher-order peaks of $g(r)$. The distinction between the finite-size effects (abrupt loss of the positional order) and the second-type disorder (monotonic deformation of the lattice) is extremely difficult on the basis of $g(r)$ but is easily obtainable from $S(q)$. The structure factors are presented in Figures 4A and 4B for, respectively, the polyhedrals and the reference spheres. Whereas the spheres are monocrystalline, the $S(q)$ for the polyhedrals is powderlike, with characteristic rings instead of sharp spots. A similar trend is observed for the impurity system and its reference

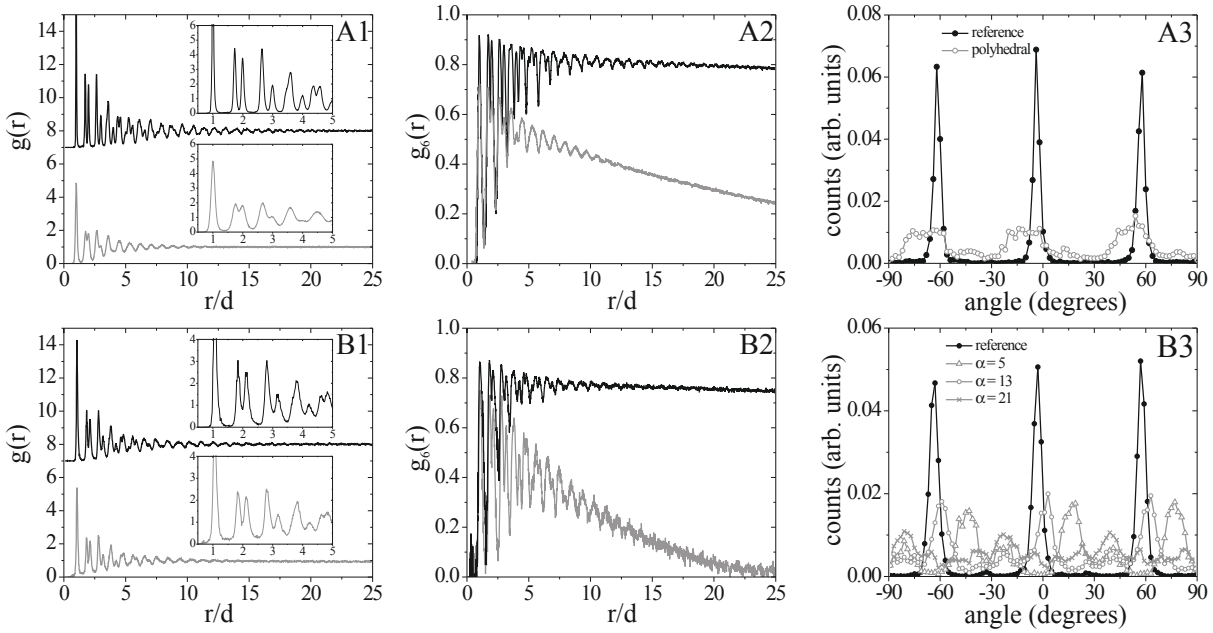

Fig. 3. (A1) Radial distribution functions $g(r)$, (A2) bond-orientational correlation functions $g_6(r)$ and angle distributions (A3) for the polyhedrals (grey) and the reference spheres (black). (B1–B3) Same as A1–A3, but now for the impurity system (grey) and the reference system without impurities (black). (B1) and (B2) $\alpha = 21$, (B3) $\alpha = 5, 13, 21$. The radial distribution functions corresponding to the reference system have been vertically shifted for clarity. The insets in (A1 and B1) show an enlargement of the first peaks of $g(r)$ to emphasize the differences between the geometrically frustrated and reference systems.

system in Figures 4D and 4E. A notable difference between the impurity system and the polyhedral system shows up in the radially averaged profiles, shown for the polyhedral system and the impurity system and their reference systems in Figures 4C and 4F respectively. As was clear from the $g(r)$ as well the positional order decays much faster in the polyhedral system. However, the angular profiles of the polyhedral system seem much wider than in the impurity system as well, which also follows from Figure 4A, where the intensity range used to depict the profile is much smaller than in Figure 4B. This seems to point to orientational changes within the grain for the polyhedral system.

The bond-orientational correlation function $g_6(r)$ is significantly affected by the polycrystallinity, as is evident from Figures 3A2 and 3B2. The bond-orientational correlation function $g_6(r)$ [60,62] is defined as

$$g_6(r) = \langle \psi_6^*(0)\psi_6(r)\rangle \tag{3}$$

with

$$\psi_6(r_i) = \frac{1}{N}\sum_{j=1}^{N} \exp[6i\theta(r_{ij})]. \tag{4}$$

Here, ψ_6 is the local bond-orientational order parameter, where the summation j runs over all, in total N, nearest neighbors of particle i. $\theta(r_{ij})$ is the angle between the bond-vector connecting particles i and j and an arbitrary fixed reference axis. The $\langle\rangle$ in equation (3) denote averaging over all pairs of particles and the index i in equation (4) runs over all particles. For both the polyhedral and the impurity system, the $g_6(r)$ decays much faster than for the reference systems, indicating that the bond-orientational correlation is gradually lost in the frustrated systems. Indeed, polycrystallinity, where every crystallite has a different orientation, is expected to destroy the bond-orientational order on a length scale comparable to the grain size. Therefore, we determined the orientational correlation length ξ_O by fitting an exponential decaying function to the envelope of $g_6(r)$: envelope of $g_6(r) \propto \exp[-r/\xi_O]$ [60,62,63]. Hence, ξ_O is a measure for the typical size of the single crystalline domains. The orientational correlation length ξ_O being approximately 18 diameters for the polyhedrals and 9 diameters for the impurity system, indeed roughly corresponds to the grain size as can be inferred from the confocal images (Figs. 2A and 2B). Interestingly, no systematical trend in the grain size as a function of the size ratio α was found, which suggests that the impurities act as immobile obstacles during the annealing of the grain boundaries. The bond-orientational correlation function of the reference systems show much slower, algebraic decay. The accompanying orientational correlation length ξ_O is more than 100 particle diameters for the reference systems, which points to the presence of long-range orientational order, i.e. large single-crystalline domains. Again, the (minimal) difference between the $g_6(r)$ of both reference systems can be attributed to the slightly different packing fraction.

Direct information about the polycrystallinity of a crystalstructure is also given by orientational profile of the structure factor [63]. In Figures 3A3 and 3B3, we show the real-space analog of this profile, that is, the distribution of angles that all nearest neighbor particles makes (with respect to an arbitrary reference axis). Clearly, in both

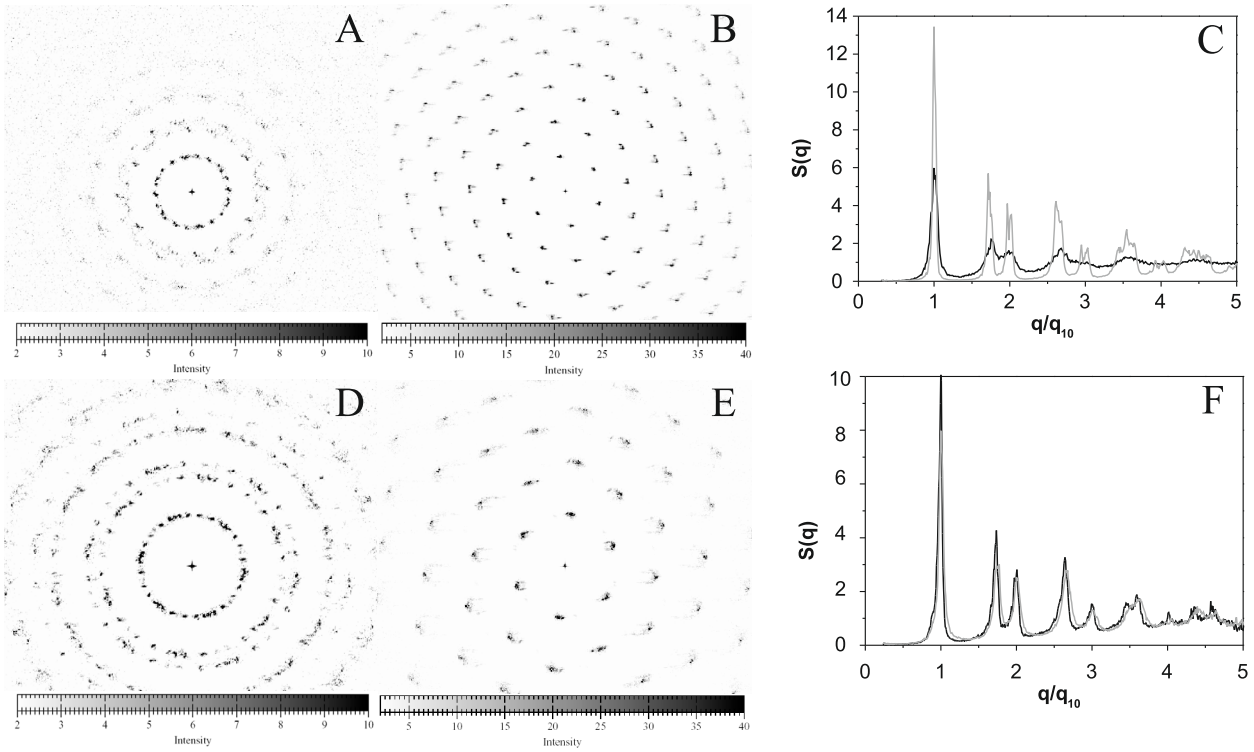

Fig. 4. The structure factor $S(\boldsymbol{q})$ for the polyhedrals (A) and the impurity system (D). The reference structure factors for both systems are shown in panels (B) and (E). The radially averaged profiles (the grey lines correspond to the reference systems) are shown in panels (C) and (F). The structure factor for the polyhedral system decays remarkably more rapidly.

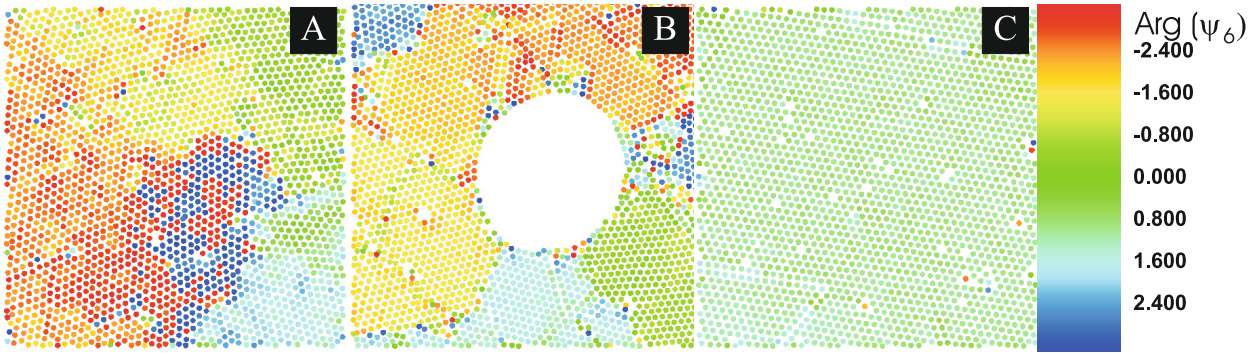

Fig. 5. (Color online) Plots of (A) the polyhedral system, (B) the impurity system and (C) the reference system. Particles are assigned a color based on their ψ_6 orientation, as indicated in the legend of panel (C). Within the grains, the reference system and the impurity system have a fairly uniform orientation, whereas the distribution of orientations within the polyhedral orientations is relatively broad.

reference systems three peaks at multiples of 60° are observed, corresponding to the three lattice orientations of a hexagonal crystal. Note that peaks with an orientational difference of 180° correspond to the same lattice orientation and are omitted for clarity. The absence of side-peaks points towards the single-crystalline structure of the reference colloidal crystals. The situation changes dramatically in the frustrated systems, where the peaks of the angle distributions are considerably broadened. Moreover, the angle distributions of the frustrated systems do not reach the zero baseline and show many other peaks. This is a direct consequence of the polycrystalline nature of the frustrated systems, as the presence of differently oriented crystalline domains results in broadening and eventually in a whole range of peaks in the angle distribution. We did not find a correlation between the orientations of the crystallites and the local curvature of the impurity, which is consistent with the absence of a relation between the grain size and the size ratio α. Note that the peaks in the angle distribution of the impurity system are generally sharper

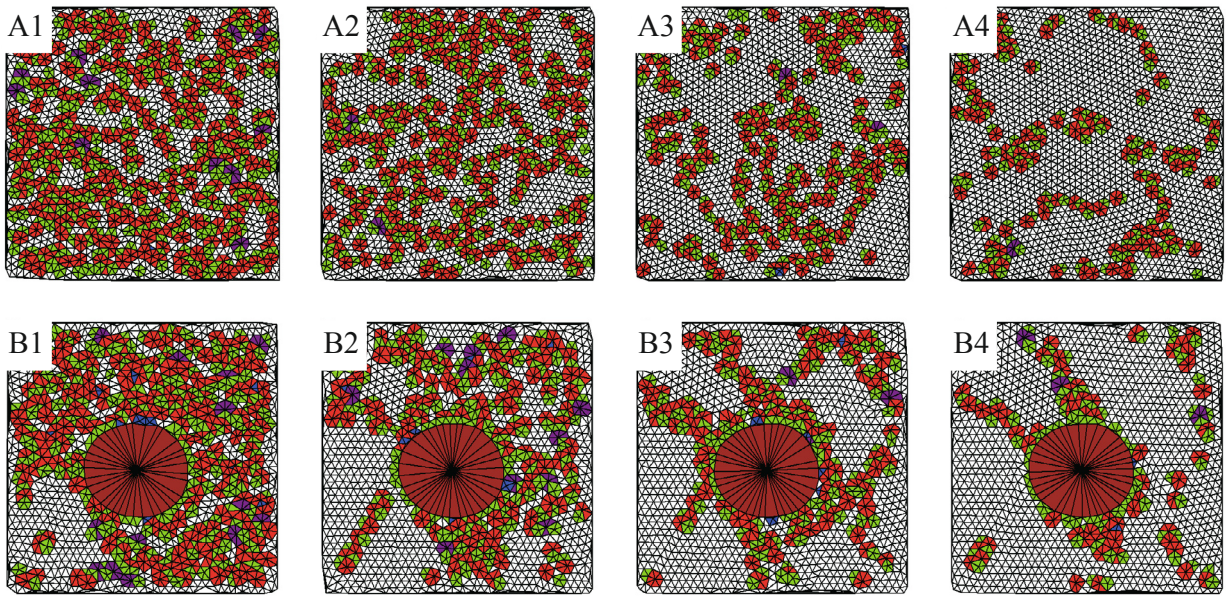

Fig. 6. (Color online) (A1–A4) Delaunay triangulations corresponding to different stages during crystallization of the polyhedral colloids (100×100 μm^2): A1–A4 respectively correspond to 0, 6, 12, 25 min after homogenization. (B1–B4) The same, but now for the impurity system with $\alpha = 13$ (60×60 μm^2): B1–B4 respectively correspond to 41, 60, 65, 80 min after homogenization. The color code for the coordination number of the particles is as follows: four-fold: blue, five-fold: green, six-fold: no color, seven-fold: red, eight-fold: purple and more than eight-fold: brown. The triangulation within the impurity has no physical meaning.

than those of the polyhedral system, which is related to the different nature of geometrical frustration in both systems: the orientation within the single grains is quite uniform in the impurity system, but changes much faster for the impurity system. This is illustrated in Figure 5, which show plots of the particle positions with colors assigned based on the local ψ_6 orientation. Within the grains, the orientation of the polyhedral sometimes changes within several color ranges, which is certainly not the case in the impurity and reference systems.

To elucidate how the grain boundaries are formed we studied the crystallization as a function of time. In Figure 6 Delaunay triangulations corresponding to different stages during crystallization are presented. The color in the triangulations corresponds to the coordination number of the particles (see caption Fig. 6). In both the polyhedral and the impurity system, crystalline regions appear (Figs. 6A1, 6B1) simultaneously in different regions of the sample. These crystallites subsequently grow (Figs. 6A2–6A4, 6B2–6B4) and meet at a certain time. Due to the random orientations of the crystallites, grain boundaries are initially formed. This rules out the scenario that an single crystallite breaks into different crystallites due to the geometrical frustration. Interestingly, the reference systems crystallize similarly as the frustrated systems, resulting in a crystal that is initially relatively rich in grain boundaries [32,59]. However, the striking difference is that in the reference systems, the grain boundaries gradually anneal in time as is evident from Figure 2C, whereas they persist in the polyhedral and impurity system on our experimental time scales (Figs. 2A and 2B) [32]. In other words, the time scale associated with the reorientation of the different crystallites – necessary to form a single crystal – is much larger for the frustrated systems than for the the reference systems.

The final structure in both systems studied here is determined by a subtle interplay between geometrical frustration, crystallization and kinetic arrest. Could it be that in the geometrically frustrated crystals the grain boundaries provide a route to minimize the stress in a similar way as the grain boundary scars that appear in a hexagonal crystal on a curved surface [29,30]? Despite their incommensurate shape, the polyhedral particles form hexagonal structures, with well defined and on average straight crystal axes [45]. Therefore, there it is unlikely that the introduction of a grain boundary reduces the stress in the crystal. However, due to the increased excluded volume with respect to a sphere, a polyhedral shape decreases the mobility of the particles, especially at high densities. As particle mobility drives the reorientation of crystallites, we argue that decreased mobility of the polyhedral particles leads to structural arrest of the crystallites, i.e. a "glass" of small, structurally arrested crystallites. The observation of vacancies and line defects (Fig. 2), which form due to the annealing of small crystallites, corroborate that the crystallization process has indeed been arrested. A similar argument can be given for the impurity system. An impurity locally introduces defects, but does not necessarily induce grain boundaries. Note that, if there exists a grain boundary, it is energetically favourable to annihilate some defects by locating the impurity in the grain boundary [19,21,63,64]. Nevertheless, the impurities

serve as immobile obstacles, which significantly slow down the reorientation-proces of the crystallites around the impurity. Consequently, this structural arrest again leads to the formation of a polycrystalline glass around the impurities.

4 Conclusions

We have shown how colloidal crystals can be used to demonstrate that two completely different ways of geometrical frustration both significantly decrease the grain size in materials. Varying particle roughness or impurity concentration may be used to tune the extent of this structural arrest. The frustration due to a polyhedral particle shape stabilizes small crystal grains on a single particle level which could be relevant for the superstructures present in powders, nanosystems and granular matter [47–49]. The frustration by the introduction of impurities stabilizes small crystallites on the single grain level, which may be used as a model system to address fundamental issues in materials science. Examples include designing highly ductile nanocrystalline materials [19–21,65–67], tackling the microscopic origin of embrittlement due to impurities [18,50] or precipitates [51,52] and understanding the high diffusivities and catalytic properties [68].

Hans Scherff and Esther Groeneveld are acknowledged for particle synthesis. This work is part of the research programme of the Stichting voor Fundamenteel Onderzoek der Materie (FOM), financially supported by the Nederlandse Organisatie voor Wetenschappelijk Onderzoek (NWO). R.P.A.D. acknowledges the Alexander von Humboldt Foundation for financial support. Support through the Transregion Sonderforschungsbereich 6 (SFB TR6) through the Deutsche Forschungsgemeinschaft (DFG) is acknowledged.

References

1. R. Phillips, *Crystals, defects and microstructure* (Cambridge University Press, Cambridge, 2001)
2. J.P. Hirth, J. Lothe, *Theory of dislocations*, 2nd edn. (Wiley, New York, 1982)
3. S.E. Offermans, N.H. van Dijk, J. Sietsma, S. Grigull, E.M. Lauridsen, L. Margulies, H.F. Poulsen, M.T. Rekveldt, S. van der Zwaag, Science **298**, 1003 (2002)
4. S. Yip, Nature **391**, 532 (1998)
5. J. Schiotz, F.D. Di Tolla, K.W. Jacobsen, Nature **391**, 561 (1998)
6. H. Van Swygenhoven, Science **296**, 66 (2002)
7. E.O. Hall, Proc. Phys. Soc. Lond. B **64**, 747 (1951)
8. N.J. Petch, J. Iron Steel Inst. **174**, 25 (1953)
9. H. Gleiter, Acta Mater. **48**, 1 (2000)
10. Q.H. Wei, X.L. Wu, Phys. Rev. E **70**, 020401(R) (2004)
11. M.J. Mills, Mater. Sci. Eng. A **166**, 35 (1993)
12. K.L. Merkle, Interface Sci. **2**, 311 (1995)
13. D.A. Muller, M.J. Mills, Mater. Sci. Eng. A **260**, 12 (1999)
14. K.L. Merkle, L.J. Thompson, Phys. Rev. Lett. **83**, 556 (1999)
15. H. Van Swygenhoven, D. Farkas, A. Caro, Phys. Rev. B **62**, 831 (2000)
16. P.M. Derlet, H. Van Swygenhoven, Phys. Rev. B **67**, 014202 (2003)
17. D. Wolf, V. Yamakov, S.R. Phillpot, A. Mukherjee, H. Gleiter, Acta Mater. **53**, 1 (2005)
18. R. Schweinfest, A.T. Paxton, M.W. Finnis, Nature **432**, 1008 (2004)
19. P.C. Millett, R.P. Selvam, S. Bansal, A. Saxena, Acta Mater. **53**, 3671 (2005)
20. P.C. Millett, R.P. Selvam, A. Saxena, Acta Mater. **54**, 297 (2006)
21. P.C. Millett, R.P. Selvam, A. Saxena, Acta Mater. **55**, 2329 (2007)
22. A. van Blaaderen, P. Wiltzius, Science **270**, 1177 (1995)
23. W.K. Kegel, A. van Blaaderen, Science **287**, 290 (2000)
24. E.R. Weeks, J.C. Crocker, A.C. Levitt, A. Schofield, D.A. Weitz, Science **287**, 627 (2000)
25. A. Pertsinidis, X.S. Ling, Nature **413**, 147 (2001)
26. S. Kodambaka, S.V. Khare, W. Swich, K. Ohmori, I. Petrov, J.E. Greene, Nature **429**, 49 (2004)
27. P. Schall, I. Cohen, D.A. Weitz, F. Spaepen, Science **305**, 1944 (2004)
28. R.P.A. Dullens, W.K. Kegel, Phys. Rev. Lett. **92**, 195702 (2004)
29. P. Lipowsky, M.J. Bowick, J.H. Meinke, D.R. Nelson, A.R. Bausch, Nat. Mater. **4**, 407 (2005)
30. T. Einert, P. Lipowsky, J. Schilling, M.J. Bowick, A.R. Bausch, Langmuir **21**, 12076 (2005)
31. A. Pertsinidis, X.S. Ling, New J. Phys. **7**, 33 (2005)
32. V.W.A. Villeneuve, R.P.A. Dullens, D.G.A.L. Aarts, E. Groeneveld, J.H. Scherff, W.K. Kegel, H.N.W. Lekkerkerker, Science **309**, 1231 (2005)
33. A.M. Alsayed, M.F. Islam, J. Zhang, P.J. Collings, A.G. Yodh, Science **309**, 1207 (2005)
34. V.W.A. Villeneuve, D. Verboekend, R.P.A. Dullens, D.G.A.L. Aarts, W.K. Kegel, H.N.W. Lekkerkerker, J. Phys.: Condens. Matter **17**, S3371 (2005)
35. P. Schall, I. Cohen, D.A. Weitz, F. Spaepen, Nature **440**, 319 (2006)
36. R.P.A. Dullens, D.G.A.L. Aarts, W.K. Kegel, Phys. Rev. Lett. **97**, 228307 (2006)
37. A. Vrij, E.A. Nieuwenhuis, H.M. Fijnaut, W.G.M. Agterhof, Faraday Discuss. Chem. Soc. **65**, 101 (1978)
38. P.N. Pusey, W. van Megen, Nature **320**, 340 (1986)
39. P.N. Pusey, in *Liquids, Freezing and the Glass Transition*, edited by J.P. Hansen, D. Levesque, J. Zinn-Justin (Elsevier, Amsterdam, 1991)
40. W. van Megen, S. Underwood, Nature **362**, 616 (1993)
41. S. Asakura, F. Oosawa, J. Chem. Phys. **22**, 1255 (1954)
42. S. Asakura, F. Oosawa, J. Pol. Sci. **33**, 183 (1958)
43. A. Vrij, Pure Appl. Chem. **48**, 471 (1976)
44. A. Yethiraj, A. van Blaaderen, Nature **421**, 513 (2003)
45. R.P.A. Dullens, M.C.D. Mourad, D.G.A.L. Aarts, J.P. Hoogenboom, W.K. Kegel, Phys. Rev. Lett. **96**, 028304 (2006)
46. R.P.A. Dullens, A.V. Petukhov, Europhys. Lett. **77**, 58003 (2007)
47. R.W. Rice, *Ceramic Fabrication Technology* (Marcel Dekker, New York, 2003)
48. N.R. Jana, Angew. Chem. Int. Ed. **43**, 1536 (2004)
49. A. Mehta, *Granular Matter: An Interdisciplinary Approach* (Springer-Verlag, New York, 1994)

50. G. Duscher, M.F. Chisholm, U. Alber, M. Rühle, Nat. Mater. **3**, 621 (2004)
51. V. Randle, B. Ralph, Acta Metall. **34**, 891 (1986)
52. J.J. Hoyt, Acta Metall. Mater. **39**, 2091 (1991)
53. R.H. Webb, Rep. Prog. Phys. **59**, 427 (1996)
54. R.P.A. Dullens, E.M. Claesson, W.K. Kegel, Langmuir **20**, 658 (2004)
55. G. Bosma, C. Pathmamanoharan, E.H.A. de Hoog, W.K. Kegel, A. van Blaaderen, H.N.W. Lekkerkerker, J. Coll. Interface Sci. **245**, 292 (2002)
56. E.H.A. de Hoog, W.K. Kegel, A. van Blaaderen, H.N.W. Lekkerkerker, Phys. Rev. E **64**, 021407 (2001)
57. R.P.A. Dullens, D.G.A.L. Aarts, W.K. Kegel, Proc. Natl. Acad. Sci. USA **103**, 529 (2006)
58. W. Schaertl, H. Sillescu, J. Stat. Phys. **77**, 1007 (1994)
59. J.P. Hoogenboom, P. Vergeer, A. van Blaaderen, J. Chem. Phys. **119**, 3371 (2003)
60. C.A. Murray, in *Bond-orientational order in condensed matter systems*, edited by K. Strandburg (Springer-Verlag, New York, 1992), pp. 137–215
61. J.C. Crocker, D.G. Grier, J. Coll. Interface Sci. **179**, 298 (1996)
62. D.R. Nelson, *Defects and geometry in condensed matter physics* (Cambridge University Press, Cambridge, 2002)
63. D.R. Nelson, M. Rubinstein, Phil. Mag. A. **46**, 105 (1982)
64. Y. Ishida, S. Okamoto, S. Hachisu, Acta Metall. **26**, 651 (1978)
65. J. Weissmüller, Nanostruct. Mater. **3**, 261 (1993)
66. C.E. Krill, R. Klein, S. Janes, R. Birringer, Mater. Sci. Forum **179–181**, 443 (1995)
67. J. Weissmüller, J. Markmann, Adv. Eng. Mat. **7**, 202 (2005)
68. C. Suryanarayana, Adv. Eng. Mat. **7**, 983 (2005)